



Automatic Quantification of Local Plaque Thickness Differences as Assessed by Serial Coronary Computed Tomography Angiography Using Scan-Quality-Based Vessel-Specific Thresholds

Finn Y. van Driest · Alexander Broersen · Rob J. van der Geest ·
J. Wouter Jukema · Arthur J. H. A. Scholte · Jouke Dijkstra

Received: September 22, 2023 / Accepted: November 3, 2023 / Published online: December 7, 2023
© The Author(s) 2023

ABSTRACT

Introduction: The use of serial coronary computed tomography angiography (CCTA) allows for the early assessment of coronary plaque progression, a crucial factor in averting major adverse cardiac events (MACEs). Traditionally, serial CCTA is assessed using anatomical landmarks to match baseline and follow-up scans. Recently, a tool has been developed that allows for the automatic quantification of local plaque thickness differences in serial CCTA utilizing plaque contour delineation. The aim of this study was to determine thresholds of plaque thickness differences that define whether there is plaque progression and/or regression. These thresholds depend on the contrast-to-noise ratio (CNR).

Prior Presentation: Parts of these contents were previously presented in the form of an e-poster at the ESC conference in Barcelona on the 27th August 2022.

F. Y. van Driest · J. Wouter Jukema ·
A. J. H. A. Scholte
Department of Cardiology, Leiden Heart-Lung
Center, Leiden University Medical Center, Leiden,
The Netherlands

A. Broersen · R. J. van der Geest · J. Dijkstra (✉)
Department of Radiology, Division of Image
Processing, Leiden University Medical Center,
Albinusdreef 2, 2333 ZA Leiden, The Netherlands
e-mail: j.dijkstra@lumc.nl

Methods: Plaque thickness differences between two scans acquired at the same moment in time should always be zero. The negative and positive differences in plaque contour delineation in these scans were used along with the CNR in order to create calibration graphs on which a linear regression analysis was performed. This analysis was conducted on a cohort of 50 patients referred for a CCTA due to chest complaints. A total of 300 coronary vessels were analyzed. First, plaque contours were semi-automatically determined for all major epicardial coronary vessels. Second, manual drawings of seven regions of interest (ROIs) per scan were used to quantify the scan quality based on the CNR for each vessel.

Results: A linear regression analysis was performed on the CNR and negative and positive plaque contour delineation differences. Accounting for the standard error of the estimate, the linear regression analysis revealed that above $1.009 - 0.002 \times \text{CNR}$ there is an increase in plaque thickness (progression), and below $-1.638 + 0.012 \times \text{CNR}$ there is a decrease in plaque thickness (regression).

Conclusion: This study demonstrates the feasibility of developing vessel-specific, quality-based thresholds for visualizing local plaque thickness differences evaluated by serial CCTA. These thresholds have the potential to facilitate the early detection of atherosclerosis progression.

Keywords: Coronary computed tomography angiography; Contrast-to-noise ratio; Coronary CT; Serial CCTA

Key Summary Points

Coronary artery disease (CAD) is still the leading cause of mortality worldwide. Early detection of CAD is imperative and holds the potential to prevent major adverse cardiac events (MACEs).

Serial coronary computed tomography angiography (CCTA) may be used for early CAD detection, but visual assessment of anatomical landmarks is used for comparing baseline and follow-up scans.

This study focused on the development of patient-specific thresholds using a cohort of 50 patients referred for a CCTA due to chest complaints. The thresholds can be applied to a recently developed tool for the automatic comparison of serial CCTA scans.

The hypothesis of this study is that patient-specific thresholds are necessary to determine plaque progression and/or regression on serial CCTA.

It was concluded that patient-specific thresholds can be determined using the contrast-to-noise ratio.

It was learned that this methodology may be used for the assessment of plaque changes on serial clinical CCTA scans.

INTRODUCTION

Coronary artery disease (CAD) is still the leading cause of mortality worldwide [1]. Early detection of CAD is imperative and holds the potential to prevent major adverse cardiac events (MACEs) [2]. There are many techniques for diagnosing CAD, one of which is coronary computed tomography angiography (CCTA).

This non-invasive imaging modality allows for both quantitative and qualitative assessments of coronary plaque. The use of serial CCTA, in which baseline and follow-up CCTA scans are compared, allows for the assessment of coronary plaque progression and/or regression [3]. The feasibility of using serial CCTA as a tool for assessing plaque changes has been demonstrated by several studies [4–6]. However, the co-registration of coronary vessels and the subsequent assessment of plaque changes between baseline and follow-up scans are still conducted manually using anatomical landmarks, as depicted in Fig. 1.

In the context of serial CCTA analysis, it is crucial that the assessment is done from a similar longitudinal viewing angle. Afterwards, coronary plaque differences are calculated based on the two-dimensional (2D) transversal view, and experts visually assess and grade the changes. However, the manual selection of viewing angles and landmarks for alignment is time consuming and potentially introduces bias [7]. Moreover, determining whether the difference in the amount of plaque thickness at a certain angle is caused by genuine changes or by a different viewing angle in the multiplanar reconstructions poses a challenge. Recently, Cao et al. developed a novel method for the automatic alignment of baseline and follow-up scans. This method enables direct visualization of plaque changes by calculating plaque thickness differences between baseline and follow-up scans from automatically delineated lumen and vessel wall contours. This tool was validated on artificial datasets. Thresholds of 0.5 mm for plaque progression and – 0.5 mm for plaque regression were found to differentiate between minor deviations and actual plaque changes [7].

The accuracy of the automatic delineation of coronary vessel and lumen contours is dependent on the scan quality, which, in turn, depends on several factors such as the image noise, movement artefacts, and numerous scan parameters [8]. Consequently, thresholds are necessary to differentiate actual changes in plaque thickness from changes caused by inaccuracies in vessel and lumen wall delineation. The scan quality on CCTA can be quantified using the contrast-to-noise ratio (CNR), as this

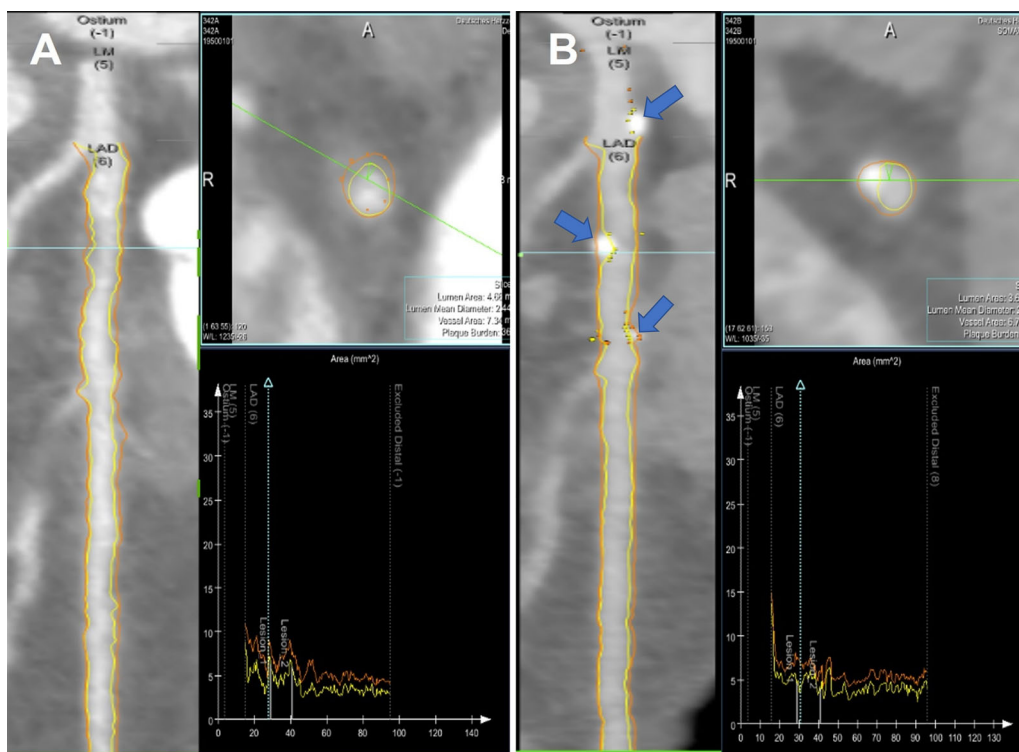


Fig. 1 Example, adapted from Weber et al. [5], of a patient who has undergone serial coronary computed tomography angiography (CCTA); the baseline scan is shown in panel **A** and the follow-up scan is shown in panel **B**. Plaque delineation is marked by the *orange and yellow lines* representing the vessel and lumen, respectively. A total

of three newly formed calcified plaques are seen in the follow-up scan, as marked by the *blue arrows*. In this case, the branching of the circumflex (*Cx*) artery may be used as an anatomical landmark for co-registration by visual analysis. *LAD* left anterior descending artery, *LM* left main artery, *mm* millimeters

can be indicative of the quality (i.e., detectability) of the contrast in the vessel of interest [9, 10]. This study aimed to use the CNR to develop vessel specific thresholds which can be used in combination with the aforementioned tool for plaque assessment on serial CCTA.

METHODS

Patients

Fifty randomly selected patients from the Leiden University Medical Center, the Netherlands, who had chest pain complaints and were referred for a CCTA were included in the current study. Two different phase reconstructions from the same scan from each patient were chosen;

the two reconstructions were in the range of either 70–80% or 30–80% for the entire cohort. In principle, this meant that plaque thickness differences should have been absent, as both phases were made almost simultaneously. The compared reconstructed phases were always within the same RR interval, which constitutes the time between two successive R waves of the QRS signal on the electrocardiogram (ECG). The compared phase pairs were always within the same gated window; either 70–80% or 30–80%, and always constituted a 75% phase and a randomly reconstructed other phase. All data were clinically acquired and retrospectively analyzed. The institutional review board of the Leiden University Medical Center, the Netherlands, approved this retrospective evaluation of clinically collected data and waived the need for written informed consent. This study was

performed in accordance with the Helsinki Declaration of 1964 and its later amendments.

Data Acquisition

CCTA was performed using a 320-row volumetric scanner (Aquilion ONE and Aquilion ONE Genesis Edition, Canon Medical Systems, Otawara, Japan). Heart rate and blood pressure were monitored 1 h before CCTA. Metoprolol (from 25 mg up to 150 mg) was administered orally to patients exceeding a heart rate of 60 beats per minute (bpm) provided that no contraindications were present. Additional metoprolol was injected intravenously if the heart rate remained above 60 bpm. Nitroglycerin (0.4 mg) was administered sublingually 4 min prior to CCTA. The scan parameters were as follows: a detector collimation of 320×0.5 mm, a 275-ms gantry rotation time, and a temporal resolution of 137 ms for the Aquilion ONE Genesis Edition; a detector collimation of 320×0.5 mm, a 350-ms gantry rotation time, and a temporal resolution of 175 ms for the Aquilion ONE. The peak tube voltage was 100–135 kV with a tube current of 140–580 mA for both scanners. 70–80% of the RR interval was scanned using prospective ECG triggering. When the heart rate was above 65 bpm, 30–80% of the RR interval was scanned. The first 50–90 ml of contrast agent (Iomeron 400, Bracco, Milan, Italy) was administered in the antecubital vein. Thereafter, 20 ml of a 1:1 mixture of contrast and saline and finally 25 ml of saline were administered. CCTA was performed at the next beat when the threshold of 300 Hounsfield units (HU) was reached in the descending aorta. The protocol settings were the same for the Aquilion ONE and Aquilion ONE Genesis Edition; a tube voltage of 100 kV was generally used. A 120-kV tube voltage was used for patients who had a weight exceeding 130 kg and/or were bearing an implantable cardioverter-defibrillator (ICD). Tube current ranged between 300 and 900 mA depending on patient size. Field of view (FOV) was also dependent on patient size and ranged between 200 and 280 mm. Image reconstruction was done using iterative reconstruction by

means of adaptive iterative dose reduction-3D (AIDR-3D) enhanced for the Aquilion ONE Genesis Edition and AIDR-3D for the Aquilion ONE using the FC03 reconstruction kernel for both scanners. Iterative reconstruction strength was set at mild, standard, or strong depending on the image noise. Image size was set at 512×512 . The slice thickness of the reconstruction was 0.25 mm for all but two of the reconstructed phases, which had a slice thickness of 1.0 mm.

It is important to note that the protocol and image reconstruction settings remained consistent for all compared reconstructed phases.

Data Processing

Dicom images were transferred to an offline workstation for analysis. Dedicated software (QAngio CT Research Edition v3.1.5.1, Medis Medical Imaging, Leiden, the Netherlands) was employed to conduct automatic tracing of the coronary arteries and the semi-automatic detection of the lumen and vessel wall contours. The contours were corrected manually if needed, whilst the reader was blinded to the results of the other phase. Coronary artery tree extraction and vessel selection are depicted in Fig. 2.

A software program developed in house by Cao et al. [7] was employed to extract the three-dimensional (3D) lumen and vessel wall surface models of the three main arteries in each of the two scans. The software co-registers both 3D models and encodes the local plaque thickness differences between the two scans on the surface of a model. Subsequently, ParaView (version 5.9.0) was utilized for the 3D visualization of the generated models.

Scan Quality

In order to quantify image quality, the CNR was calculated separately for the left anterior descending artery (LAD), the right coronary artery (RCA), and the circumflex artery (Cx). We opted to use CNR as a metric to quantify image quality as this has been proven to affect the accuracy of CCTA. Furthermore, it has been

demonstrated that a reduced CNR results in a reduced sharpness of vessel visualization. The latter negatively influences plaque visualization and thus also software-aided plaque delineation [11, 12]. Contrary to the signal-to-noise ratio (SNR), CNR serves as a quantitative metric for low-contrast lesion detection: the higher the CNR between lesion and background, the more likely the detection of the lesion [13]. Although the SNR and CNR formulas are similar, SNR lacks specificity, as it does not consider the mean intensity of the surrounding epicardial tissue [14]. Therefore, CNR presents superior significance in contrast-enhanced scans like CCTA, as it is a measure of image quality based on a contrast [15]. A total of seven regions of

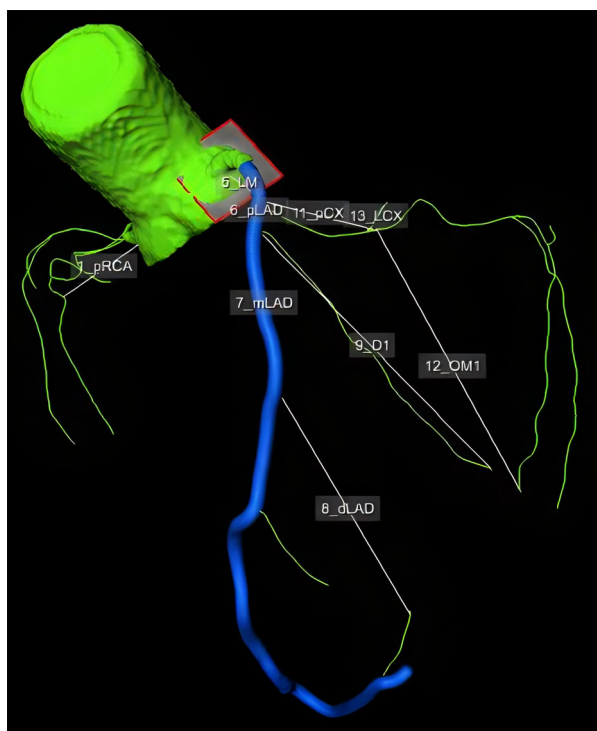


Fig. 2 The complete coronary tree is extracted from the CCTA. In this example, the left anterior descending artery (LAD) is marked in *blue* for performing plaque delineation. *LM* left main artery, *pLAD* proximal left anterior descending artery, *dLAD* distal left anterior descending artery, *pRCA* proximal right coronary artery, *pCX* proximal circumflex artery, *LCX* left circumflex artery, *D1* first diagonal artery, *OM1* first obtuse marginal artery, *mLAD* mid left anterior descending artery, *CCTA* coronary computed tomography angiography

interest (ROIs) per patient were defined for the measurement of the intensity values and the subsequent calculation of the CNR. The first ROI was placed in the ascending aorta, superior and in close proximity to the origin of the RCA, to define image noise. Thereafter, three ROIs were placed in the most proximal part of each coronary vessel. The final three ROIs were placed in the epicardial tissue surrounding each vessel, adhering to the same slice position and in spatial proximity to the ROI in the corresponding vessel. ROI placement was performed meticulously to exclude calcifications, plaques, vessel walls, and any potential image artifacts. Figure 3 depicts an example of a patient with ROIs placed in the aorta, LAD, and surrounding epicardial tissue.

The CNR was subsequently calculated for each vessel using the following formula:

$$\text{CNR} = \frac{\mu_{\text{vessel}} - \mu_{\text{epicardial tissue}}}{\sigma_{\text{aorta}}},$$

in which μ_{vessel} represents the mean HU intensity of the specific coronary vessel, $\mu_{\text{epicardial tissue}}$ represents the mean HU intensity of the epicardial tissue in spatial proximity to the specific coronary vessel, and σ_{aorta} represents the standard deviation of the HU intensity in the ascending aorta.

Negative and Positive Thresholds

Coronary lumen and vessel wall contours are detected in the multi-planar reformatted images of the artery. Based on the detected lumen and vessel wall contours, the plaque thickness at a certain location in an artery can be calculated. This is done by calculating the distance between the points at which the lumen contour and the vessel contour intersect with the line through the lumen center. The change in plaque thickness is determined as the difference in plaque thickness at the corresponding location between scans [7]. It is important to note that the accuracy of contours and thus plaque delineation is dependent on the scan quality [16]. Therefore, thresholds are needed to filter out insignificant changes in plaque thickness

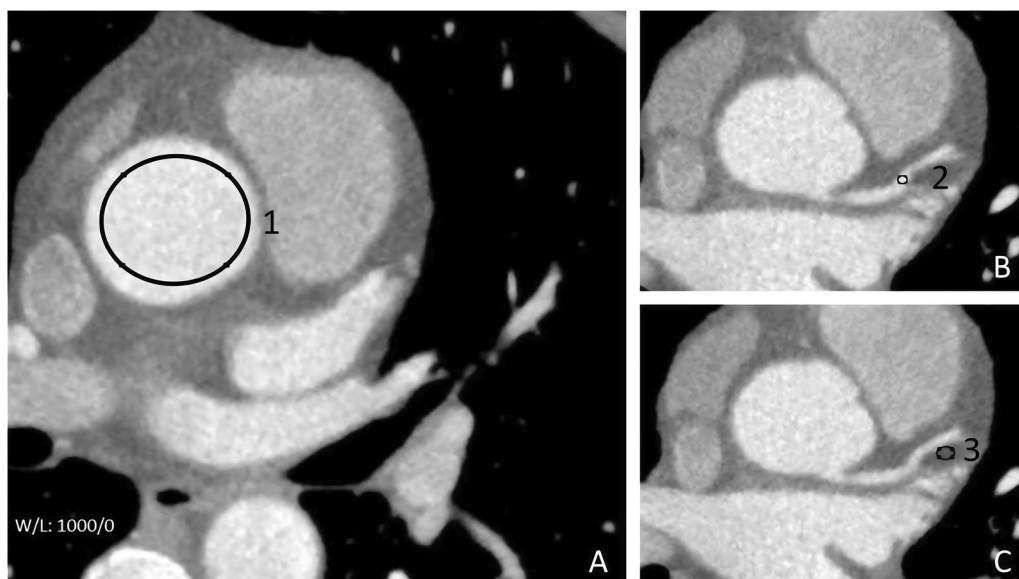


Fig. 3 Regions of interest are manually drawn in the aorta (A), proximal LAD (B), and the corresponding epicardial tissue surrounding the LAD (C). This means of operation

is the same for the Cx and the RCA. *LAD* left anterior descending artery, *Cx* circumflex artery, *RCA* right coronary artery

differences resulting from variations in contour quality. Figure 4 depicts a clinical example of a case with plaque progression in the LAD that shows the importance of using thresholds for plaque thickness change visualization.

In order to establish vessel-specific thresholds, calibration graphs were created between the lowest measured CNR of a vessel in both phases and the largest negative and largest positive differences in plaque thickness measurements between two-phase scans. For each patient, two different reconstructed phases from the same scan were compared. As plaque differences between two reconstructed phases from the same scan and from the same patient should always be zero, it is possible to compare both phases in a two-way manner. Hence, for each patient, two values of the plaque thickness difference were obtained, yielding a total of 100 values. Subsequently, any plaque thickness delineation differences between two-phase scan sets had to be attributable to different factors such as scan quality. The software tool from Cao et al. [7] was utilized for automatically calculating the negative and positive plaque thickness differences. Subsequently, the largest negative and largest positive thickness

differences were plotted against the vessel-specific CNR. Linear regression facilitates the determination of the linear relationship between a dependent and independent variable, in this case plaque thickness difference and CNR, respectively. Formulas were derived through linear regression analysis conducted on the aforementioned charts using SPSS software (version 25, SPSS IBM Corp., Armonk, New York). The standard error of the estimate which is used in linear regression analysis was multiplied by a value of one instead of the customary two. This was done pragmatically in order to ensure that the model was capable of detecting relatively small plaque changes with regard to the average coronary lumen diameter, which is between 3 and 4 mm [17]. A detailed step-by-step flowchart depicting the aforementioned process is presented in Fig. 5.

Inter-observer Measurements

A random set of 15 scans were utilized for inter-observer measurements, resulting in the analysis of 45 coronary vessels. Observer AB (with 13 years of experience in cardiovascular image analysis) also drew a total of seven ROIs per

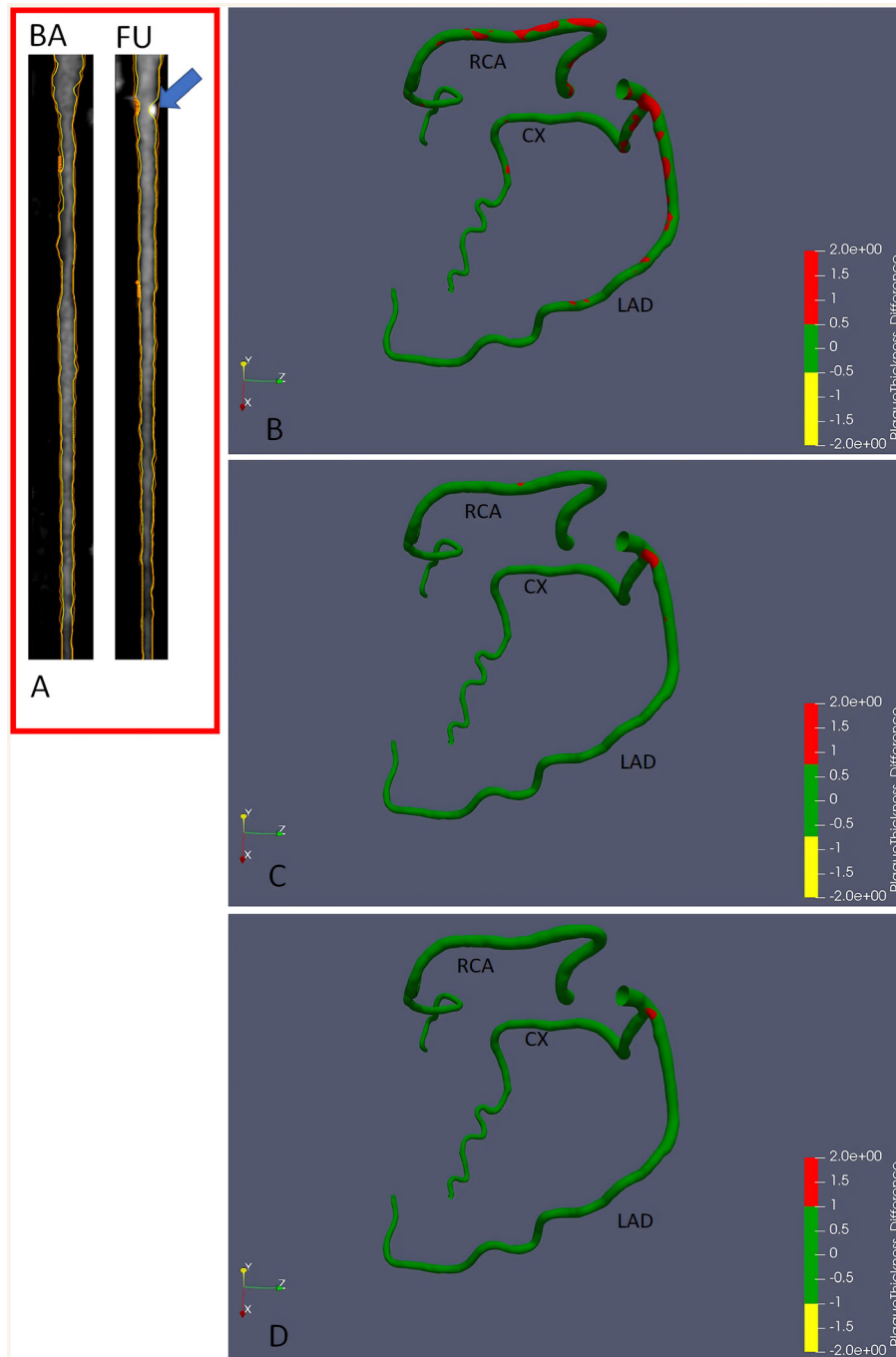


Fig. 4 A newly formed plaque is observed in the proximal LAD, as marked by the *blue arrow* (A). No other vessels have plaque (changes). Multiple areas are identified as having plaque progression using cutoff values of -0.5 and 0.5 (B). Larger cutoff values of -0.75 and 0.75 still do not allow plaque progression to be discerned in the RCA and the middle part of the LAD, as marked by the *red areas* (C). Finally, cutoff values of -1.0 and 1.0 seem to

correlate well with the visual observations in panel A (D). This demonstrates the importance of using cutoff values, yet the adaptive values must still be calculated using the CNR as a marker of scan quality. Plaque thickness differences are given in mm. BA baseline, FU follow-up, RCA right coronary artery, LAD left anterior descending artery, Cx circumflex artery, CNR contrast-to-noise ratio

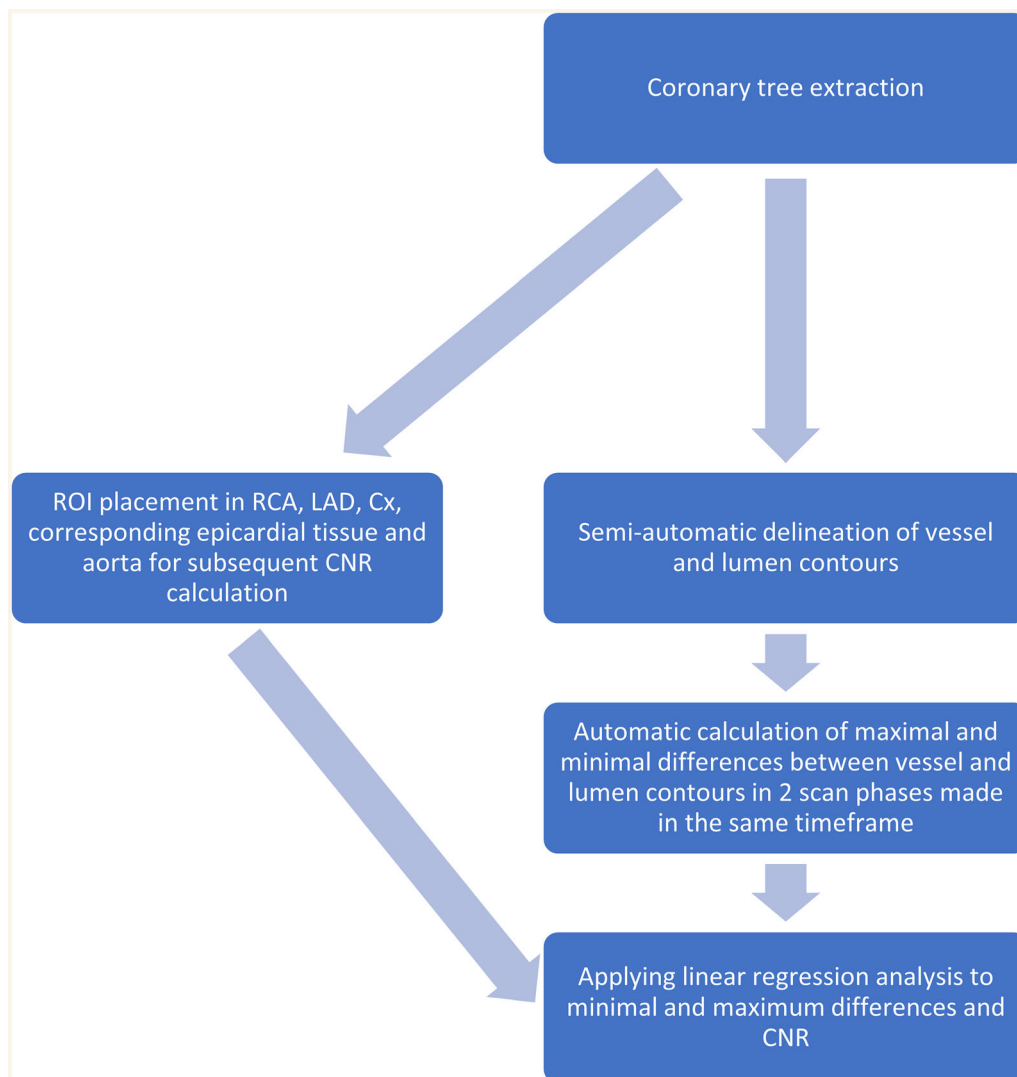


Fig. 5 Flowchart depicting the process of creating formulas for thresholds of plaque differences using scan quality. *ROI* region of interest, *CNR* contrast-to-noise ratio, *RCA*

right coronary artery, *LAD* left anterior descending artery, *Cx* circumflex artery

patient for *CNR* measurements. Thereafter, the calculated *CNR* values were compared to those obtained by observer FY (with 3 years of experience in cardiovascular image analysis). Subsequently, correlations were tested using Pearson's correlation coefficient.

RESULTS

A total of 300 coronary vessels were used for the current analysis. The average *CNR* value was

13.4 ± 3.6 . The average positive and negative differences in measured plaque thickness were 0.7 ± 0.3 and -0.9 ± 0.6 mm, respectively. A more detailed description of the values per vessel is depicted in Table 1.

A trend was observed for the relationship between the higher and lower *CNR* values and the subsequent positive and negative plaque thickness differences, as depicted in Figs. 6 and 7.

A linear regression analysis was performed for all the positive and negative differences in

Table 1 Detailed description of the values found per vessel. All values are the mean ± standard deviation

	Mean CNR	Mean positive difference	Mean negative difference
LAD	13.3 ± 3.6	0.6 ± 0.4 mm	− 0.8 ± 0.6 mm
RCA	13.7 ± 3.6	0.7 ± 0.4 mm	− 1.0 ± 0.6 mm
Cx	13.3 ± 3.5	0.5 ± 0.2 mm	− 0.8 ± 0.6 mm

CNR contrast-to-noise-ratio, LAD left anterior descending artery, RCA right coronary artery, Cx circumflex artery, Mm millimeters

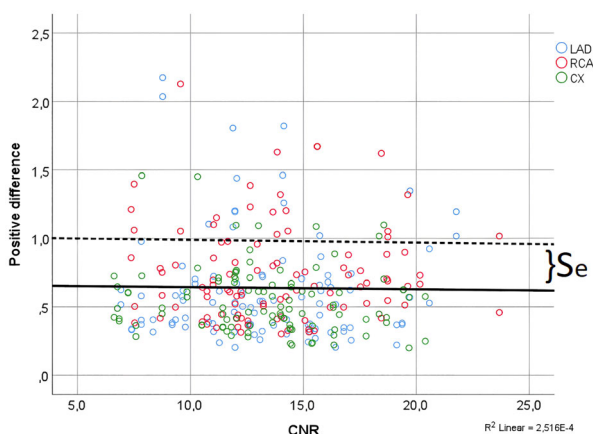


Fig. 6 Positive differences in plaque thickness are plotted against the respective CNR of the specific vessel. The dotted line represents the relationship between CNR and positive difference including the standard error of the estimate. A trend is observed in which higher CNR values (related to higher scan quality) and lower CNR values (related to lower scan quality) correspond to lower and higher positive differences in plaque thickness, respectively. Positive differences are given in mm. *Se* standard error of the estimate, LAD left anterior descending artery, RCA right coronary artery, Cx circumflex artery, CNR contrast-to-noise ratio

plaque thickness along with the CNR calculated per vessel. Along with the standard errors of the estimate—which were 0.349 and − 0.61, respectively, for the positive and negative differences—this analysis yielded the following formulas:

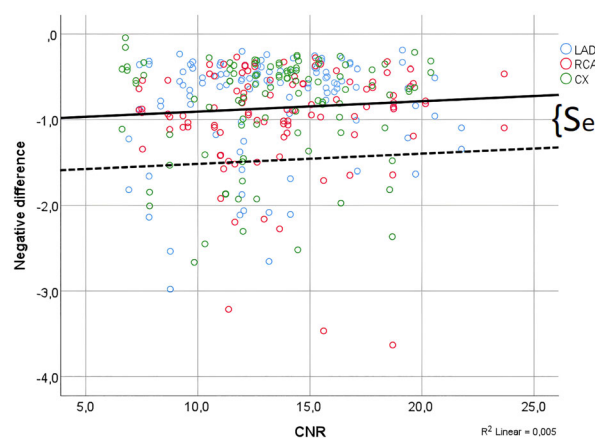


Fig. 7 Negative differences in plaque thickness are plotted against the respective CNR of the specific vessel. The dotted line represents the relationship between CNR and negative difference including the standard error of the estimate. A trend is observed in which higher CNR values (related to higher scan quality) and lower CNR values (related to lower scan quality) correspond to higher and lower negative differences in plaque thickness, respectively. Negative differences are given in mm. *Se* standard error of the estimate, LAD left anterior descending artery, RCA right coronary artery, Cx circumflex artery, CNR contrast-to-noise ratio

$$\text{Positive difference} = (0.660 - (0.002 \times \text{CNR})) + 0.349$$

$$\text{Negative difference} = (-1.028 + (0.012 \times \text{CNR})) - 0.61.$$

Positive and negative plaque thickness differences are expressed in mm.

The inter-observer correlation for CNR values was excellent, with a correlation coefficient of 0.872 ($p < 0.001$). Figure 8 demonstrates the correlation between CNR measurements done by observers FY and AB.

The application of the aforementioned formulas along with the corresponding thresholds is shown in the two examples depicted in Figs. 9 and 10. It is important to emphasize that a distinct threshold was applied for each vessel, which was determined from the lowest CNR observed in that vessel across both the baseline and the follow-up scans.

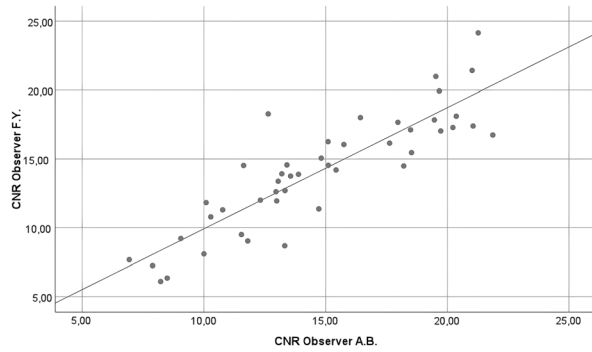


Fig. 8 Correlation between CNR measurements done by observers FY and AB. *CNR* contrast-to-noise ratio

DISCUSSION

In this study, we have proposed a method for the objective assessment of plaque dynamics using patient-specific thresholds on CCTA. These thresholds were obtained by using calibration graphs with two-phase scan sets in which negative and positive plaque thickness

differences were plotted against the subsequent scan quality calculated as the CNR. The results demonstrate that the use of these vessel-specific thresholds allows for the direct visualization and quantification of plaque thickness differences, and they show good visual agreement with the plaque localization. It is important to stress that although there is no gold standard for plaque change validation in the current study, an artificial validation of the proposed method was done by Cao et al. Their study demonstrated excellent correspondence between calculated plaque differences and artificially created plaque changes in coronary arteries [7].

Calibration graphs and a subsequently performed linear regression yielded a very slight trend regarding the CNR and negative and positive plaque thickness differences. Further analysis of these formulas reveals that changes in CNR only mildly affect the subsequent threshold. Positive and negative plaque thickness thresholds of 0.982 mm and -1.472 mm

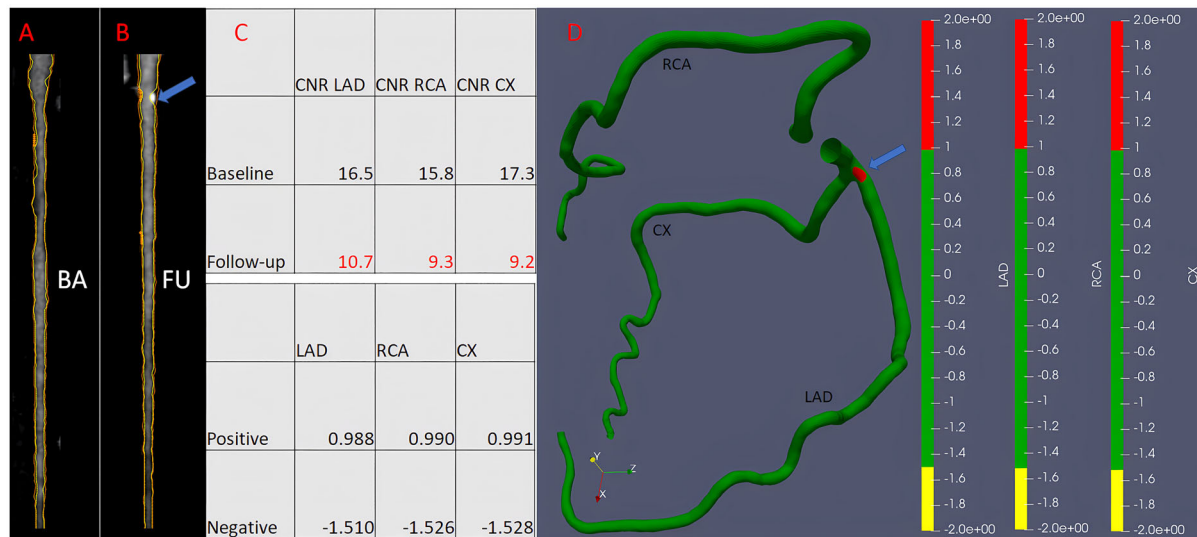


Fig. 9 Patient with a newly formed calcified plaque only in the proximal LAD after 7 years follow-up, as marked by the *blue arrow* (A and B). The CNR was calculated separately for the LAD, RCA, and Cx. CNR values of 10.7, 9.3, and 9.2 were found for those vessels, respectively (C). Using the aforementioned CNR values, thresholds (positive and negative) were calculated for each vessel

separately. Subsequent visualization of the coronary tree with those thresholds clearly demonstrates the plaque change in the proximal LAD, as marked by the *red area* and *blue arrow* (D). Plaque thickness differences are given in mm. *BA* baseline, *FU* follow-up, *RCA* right coronary artery, *LAD* left anterior descending artery, *Cx* circumflex artery, *CNR* contrast-to-noise ratio

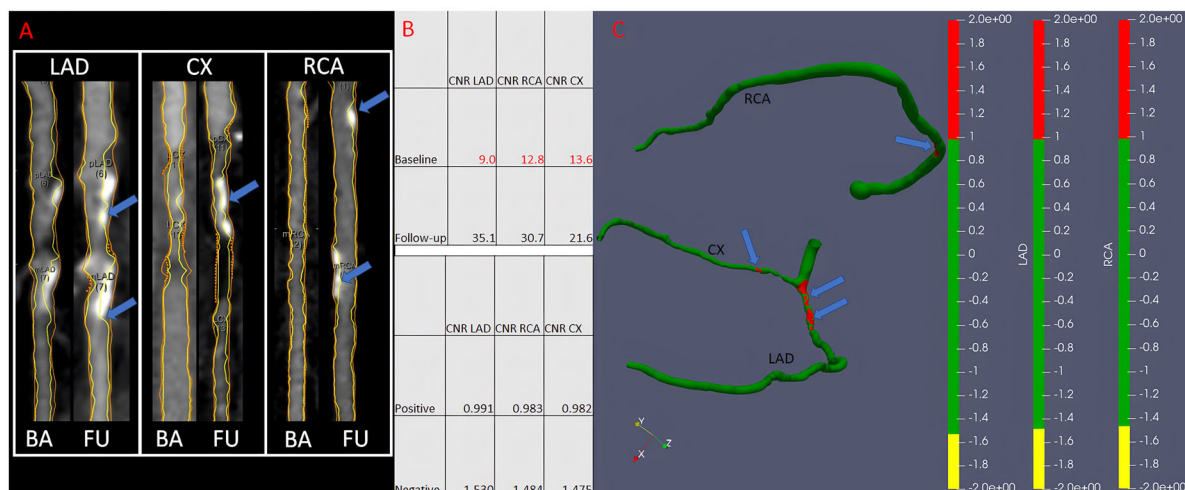


Fig. 10 Patient with newly formed plaques in the LAD, Cx, and RCA, as marked by the *blue arrows*, after 6 years of follow-up (A). The CNR was calculated separately for the LAD, RCA, and Cx. CNR values of 9.0, 12.8, and 13.6 were found for those vessels, respectively (B). Using the aforementioned CNR values, thresholds (positive and negative) were calculated for each vessel separately. Subsequent visualization of the coronary tree with those thresholds clearly demonstrates the plaque changes in the

LAD, Cx, and RCA, as marked by the *red areas* and *blue arrows* (C). Note that the newly formed plaque in the proximal RCA is not visualized as it is on the opposite side of the vessel. This is also the case with the Cx: a major part of the newly formed plaque is on the opposite side of the vessel. Plaque thickness differences are given in mm. BA baseline, FU follow-up, RCA right coronary artery, LAD left anterior descending artery, Cx circumflex artery, CNR contrast-to-noise ratio

are found, respectively, if we utilize the average CNR value of 13.4. Previous studies by Fayad et al. indicate that the average vessel wall thickness ranges from 0.75 ± 0.17 mm for healthy segments to an average thickness range of 4.38 ± 0.71 mm for large plaques causing stenosis of $\geq 40\%$ [18]. The positive and negative plaque thickness thresholds found in our study using the average CNR would be clinically applicable as they fall in between the range of values for healthy and atherosclerotic segments found by Fayad et al.

The inter-observer correlation for CNR values was excellent. Hence, differences in ROI placement caused by inter-observer variability will only have a very minor impact on the final formulas. Furthermore, Papadopoulou et al. demonstrated that inter-observer agreement for the detection of atherosclerotic segments using plaque delineation was strong (Cohen’s kappa coefficient $K = 1.0$) [19]. This is especially important, as the detection of serial plaque changes is dependent on the plaque delineation in subsequent baseline and follow-up scans.

A great advantage of the proposed method for the assessment of serial plaque changes, as opposed to the current method based on the calculation of the plaque’s volume, is that changes can be visualized locally. Furthermore, our method of visualizing plaque differences is not affected by the size of the vessel, which is an advantage compared to the current method [20–22]. Visualizing the location(s) of plaque changes in the subsequent coronary vessel(s) may be especially beneficial for patients undergoing coronary catheterization as this can guide clinicians to the location(s) of interest.

Limitations

This study has several limitations which are innate to its novel nature and retrospective design. A major limitation is the absence of a gold standard for the assessment of plaque changes aside from visual assessment. For the analyzed patient population, no intravascular imaging like intravascular ultrasound (IVUS)

was available to serve as a high-resolution ground truth. As thresholds are used in the output 3D model, there is a possibility of “missing” plaque changes that are below the threshold, and unfortunately there is no method to objectify this possibility. Contrastingly, there is also a chance of “exaggerating” plaque changes if the lumen or vessel wall is incorrectly delineated. The use of one times the standard error instead of the more conventionally used two times its value will statistically also lead to more false-positive plaque changes, as the confidence interval is then set at around 68%, in contrast to the “regular” 95%. On the other hand, having relatively low negative and high positive thresholds as compared to the average coronary lumen size would lead to more false negatives [17]. Ultimately, we used one standard error from a pragmatic perspective, as this would ensure the detection of relatively small plaque changes. Furthermore, despite not having a gold standard for plaque change validation, plaque changes that are potentially wrongfully detected may be dismissed, as visual assessment remains a form of ground truth. The CNR was calculated at the proximal part of the vessel. However, CNR values can change upon moving more distally in the subsequent vessel, as was demonstrated by Yokota et al. Fortunately, the differences between proximal and distal locations were found to be small [23]. Yet, the possibility that plaque thickness delineation is affected by the location in the vessel cannot be excluded. Also, the CNR itself is very sensitive to the background location in the epicardium, which leads to biased inter-observer measurements. The correlation coefficient found for inter-observer correlations regarding CNR measurements was very strong. The vast majority of the reconstructed phases had a slice thickness of 0.25 mm, yet two phases were reconstructed using a 1.0-mm slice thickness. A study by Alshipli and Kabir has demonstrated that the effect of slice thickness on image noise is extremely minor [24]. Furthermore, it is worth noting that 98% of our cohort utilized a 0.25-mm slice thickness; they greatly outnumber the 2% that was reconstructed based on a 1.0-mm slice thickness. Hence, a potential bias

caused by these slice thickness differences would be highly unlikely.

Finally, it must be noted that although the demonstrated method may visualize plaque differences locally, it is often more effective to determine the total plaque burden with regard to the management of patients with CAD. This is due to the fact that atherosclerosis is a dynamic process that changes constantly. Hence, placing emphasis on the entire atherosclerosis process and global imaging of the heart represent a better approach than focusing on a single plaque [25]. Also, a recent development has been the use of positron emission tomography (PET) using ^{18}F -NaF, which has the ability to detect the active microcalcification that is believed to represent unstable plaques. This is contrary to computed tomography (CT) scans, which detect macrocalcifications, as these represent stable areas where the atherosclerotic disease is quiescent [26].

As the goal of this study was to develop vessel-specific thresholds for the direct visualization of plaque thickness differences, more testing and further investigation are needed.

CONCLUSION

The development of patient-specific plaque thickness thresholds seems feasible and allows for the direct visualization of plaque thickness differences in serial CTA, as demonstrated by these preliminary results. However, currently this study must be interpreted as a proof of concept for determining and using threshold values for clinical data. In the future this methodology may be used for the assessment of plaque changes on serial clinical CCTA scans, preferably combined with serial IVUS acquisition or a thorough cardiac phantom study.

ACKNOWLEDGEMENTS

Medical Writing/Editorial Assistance We would like to express our sincere thanks to Jip R.A. Schoenaker for providing help

with the editing of the figures. We would like to express our sincere thanks to Grazia Iaffaldano for helping with the spelling and grammar of the English text. There was no funding for this editorial assistance.

Author Contributions. Finn Y. van Driest: concept and design, statistical analysis, drafting the manuscript. Alexander Broersen: drafting the manuscript, performing inter-observer measurements, providing help with the software developed in house. Rob J. van der Geest: drafting the manuscript. Jouke Dijkstra: drafting the manuscript. Arthur J.H.A. Scholte: drafting the manuscript. J. Wouter Jukema: drafting the manuscript.

Funding. The project LSHM19028 PRAGMATICS, is co-funded by the PPP Allowance made available by Health~Holland, Top Sector Life Sciences & Health, to stimulate public-private partnerships. No funding or sponsorship was received for the publication of this article.

Data Availability. The datasets generated during and/or analyzed during the current study are available from the corresponding author on reasonable request.

Declarations

Conflict of Interest. Finn Y. van Driest, Alexander Broersen, Rob J. van der Geest, Jouke Dijkstra, Arthur J.H.A. Scholte, and J. Wouter Jukema state that they have no relevant conflicts of interest to disclose.

Ethical Approval. All data were clinically acquired and retrospectively analyzed. The institutional review board of the Leiden University Medical Center, the Netherlands, approved this retrospective evaluation of clinically collected data and waived the need for written informed consent. This study was performed in accordance with the Helsinki Declaration of 1964 and its later amendments.

Open Access. This article is licensed under a Creative Commons Attribution-NonCommercial 4.0 International License, which permits any non-commercial use, sharing,

adaptation, distribution and reproduction in any medium or format, as long as you give appropriate credit to the original author(s) and the source, provide a link to the Creative Commons licence, and indicate if changes were made. The images or other third party material in this article are included in the article's Creative Commons licence, unless indicated otherwise in a credit line to the material. If material is not included in the article's Creative Commons licence and your intended use is not permitted by statutory regulation or exceeds the permitted use, you will need to obtain permission directly from the copyright holder. To view a copy of this licence, visit <http://creativecommons.org/licenses/by-nc/4.0/>.

REFERENCES

1. Mackay J, Mensah G, Mendis S, Greenland K. The atlas of heart disease and stroke. Geneva: World Health Organization; 2004.
2. Bom MJ, van der Heijden DJ, Kedhi E, van der Heyden J, Meuwissen M, Knaapen P, et al. Early detection and treatment of the vulnerable coronary plaque: can we prevent acute coronary syndromes? *Circ Cardiovasc Imaging*. 2017;10(5): 005973.
3. Hoffmann U, Moselewski F, Nieman K, Jang IK, Ferencik M, Rahman AM, et al. Noninvasive assessment of plaque morphology and composition in culprit and stable lesions in acute coronary syndrome and stable lesions in stable angina by multidetector computed tomography. *J Am Coll Cardiol*. 2006;47(8):1655–62.
4. Yu M, Li W, Lu Z, Wei M, Yan J, Zhang J. Quantitative baseline CT plaque characterization of unrevascularized non-culprit intermediate coronary stenosis predicts lesion volume progression and long-term prognosis: a serial CT follow-up study. *Int J Cardiol*. 2018;264:181–6.
5. Weber C, Deseive S, Brim G, Stocker TJ, Broersen A, Kitslaar P, et al. Coronary plaque volume and predictors for fast plaque progression assessed by serial coronary CT angiography—a single-center observational study. *Eur J Radiol*. 2020;123: 108805.
6. Lee SE, Sung JM, Andreini D, Al-Mallah MH, Budoff MJ, Cademartiri F, et al. Differences in progression to obstructive lesions per high-risk plaque features and plaque volumes with CCTA. *JACC Cardiovasc Imaging*. 2020;13(6):1409–17.

7. Cao Q, Broersen A, Kitslaar PH, Yuan M, Lelieveldt BPF, Dijkstra J. Automatic coronary artery plaque thickness comparison between baseline and follow-up CCTA images. *Med Phys*. 2020;47(3):1083–93.
8. Ghekiere O, Salgado R, Buls N, Leiner T, Mancini I, Vanhoenacker P, et al. Image quality in coronary CT angiography: challenges and technical solutions. *Br J Radiol*. 2017;90(1072):20160567.
9. Welvaert M, Rosseel Y. On the definition of signal-to-noise ratio and contrast-to-noise ratio for fMRI data. *PLoS ONE*. 2013;8(11): e77089.
10. Konstantinidis A. 2.02—Physical parameters of image quality. In: Brahme A, editor. *Comprehensive biomedical physics*. Oxford: Elsevier; 2014. p. 49–63.
11. Hubbard L, Malkasian S, Zhao Y, Abbona P, Molloy S. Contrast-to-noise ratio optimization in coronary computed tomography angiography: validation in a swine model. *Acad Radiol*. 2019;26(6):e115–25.
12. Cademartiri F, Mollet NR, Lemos PA, Saia F, Midiri M, de Feyter PJ, et al. Higher intracoronary attenuation improves diagnostic accuracy in MDCT coronary angiography. *AJR Am J Roentgenol*. 2006;187(4):W430–3.
13. Hendrick RE. Signal, noise, signal-to-noise and contrast-to-noise ratios. In: *Breast MRI: fundamentals and technical aspects*. New York: Springer New York; 2008. p. 93–111.
14. Feger S, Rief M, Zimmermann E, Martus P, Schuijff JD, Blobel J, et al. The impact of different levels of adaptive iterative dose reduction 3D on image quality of 320-row coronary CT angiography: a clinical trial. *PLoS ONE*. 2015;10(5): e0125943.
15. Alsleem HA, Almohiy HM. The feasibility of contrast-to-noise ratio on measurements to evaluate CT image quality in terms of low-contrast detailed detectability. *Med Sci (Basel)*. 2020;8(3):26.
16. Ghanem AM, Hamimi AH, Matta JR, Carass A, Elgarf RM, Gharib AM, et al. Automatic coronary wall and atherosclerotic plaque segmentation from 3D coronary CT angiography. *Sci Rep*. 2019;9(1):47.
17. Dodge JT Jr, Brown BG, Bolson EL, Dodge HT. Lumen diameter of normal human coronary arteries. Influence of age, sex, anatomic variation, and left ventricular hypertrophy or dilation. *Circulation*. 1992;86(1):232–46.
18. Fayad ZA, Fuster V, Fallon JT, Jayasundera T, Worthley SG, Helft G, et al. Noninvasive in vivo human coronary artery lumen and wall imaging using black-blood magnetic resonance imaging. *Circulation*. 2000;102(5):506–10.
19. Papadopoulou S-L, Neeffjes LA, Schaap M, Li H-L, Capuano E, van der Giessen AG, et al. Detection and quantification of coronary atherosclerotic plaque by 64-slice multidetector CT: a systematic head-to-head comparison with intravascular ultrasound. *Atherosclerosis*. 2011;219(1):163–70.
20. Nakanishi R, Alani A, Matsumoto S, Li D, Fahmy M, Abraham J, et al. Changes in coronary plaque volume: comparison of serial measurements on intravascular ultrasound and coronary computed tomographic angiography. *Tex Heart Inst J*. 2018;45(2):84–91.
21. Inoue K, Motoyama S, Sarai M, Sato T, Harigaya H, Hara T, et al. Serial coronary CT angiography-verified changes in plaque characteristics as an end point: evaluation of effect of statin intervention. *JACC Cardiovasc Imaging*. 2010;3(7):691–8.
22. Foldyna B, Lo J, Mayrhofer T, Grinspoon SK, Hoffmann U, Lu MT. Individual coronary plaque changes on serial CT angiography: within-patient heterogeneity, natural history, and statin effects in HIV. *J Cardiovasc Comput Tomogr*. 2020;14(2):144–8.
23. Yokota Y, Takeda C, Kidoh M, Oda S, Aoki R, Ito K, et al. Effects of deep learning reconstruction technique in high-resolution non-contrast magnetic resonance coronary angiography at a 3-tesla machine. *Can Assoc Radiol J*. 2020;72(1):120–7.
24. Alshipli M, Kabir NA. Effect of slice thickness on image noise and diagnostic content of single-source-dual energy computed tomography. *J Phys: Conf Ser*. 2017;851(1): 012005.
25. Høiland-Carlsen PF, Piri R, Gerke O, Edenbrandt L, Alavi A. Assessment of total-body atherosclerosis by PET/computed tomography. *PET Clin*. 2021;16(1): 119–28.
26. Bassir A, Raynor WY, Park PSU, Werner TJ, Alavi A, Revheim M-E. Molecular imaging in atherosclerosis. *Clin Transl Imaging*. 2022;10(3):259–72.